4-20-2008

The Effect of 53 μm IR Radiation on 18 cm OH Megamaser Emission

Philip Lockett
Centre College

Moshe Elitzur
University of Kentucky, moshe@pa.uky.edu

The Effect of 53 μm IR Radiation on 18 cm OH Megamaser Emission

Notes/Citation Information
Published in *The Astrophysical Journal*, v. 677, no. 2, p. 985-992.

Digital Object Identifier (DOI)
http://dx.doi.org/10.1086/533429

The Astrophysical Journal, 677:985–992, 2008 April 20

THE EFFECT OF 53 μm IR RADIATION ON 18 cm OH MEGAMASER EMISSION

Philip Lockett[1] and Moshe Elitzur[2]
Received 2007 October 5; accepted 2008 January 9

ABSTRACT

OH megamasers (OHMs) emit primarily in the main lines at 1667 and 1665 MHz and differ from their Galactic counterparts due to their immense luminosities, large line widths, and 1667/1665 MHz flux ratios, which are always greater than 1. We find that these maser properties result from strong 53 μm radiative pumping combined with line overlap effects caused by turbulent line widths $\sim$20 km s^{-1}; pumping calculations that do not include line overlap are unreliable. A minimum dust temperature of $\sim$45 K is needed for inversion, and maximum maser efficiency occurs for dust temperatures $\sim$80–140 K. We find that warmer dust can support inversion at lower IR luminosities, in agreement with observations. Our results are in good agreement with a clumpy model of OHMs, with clouds sizes $\lesssim$1 pc and OH column densities $\sim 5 \times 10^{16}$ cm^{-2}, that is able to explain both the diffuse and compact emission observed for OHMs. We suggest that *all* OH main-line masers may be pumped by far-IR radiation, with the major differences between OHMs and Galactic OH masers caused by differences in line width produced by line overlap. Small Galactic maser line widths tend to produce stronger 1665 MHz emission. The large OHM line widths lead to inverted ground-state transitions having approximately the same excitation temperature, producing 1667/1665 MHz flux ratios greater than 1 and weak satellite line emission. Finally, the small observed ratio of pumping radiation to dense molecular gas, as traced by HCN and HCO$^+$, is a possible reason for the lack of OH megamaser emission in NGC 6240.

Subject headings: galaxies: starburst — masers — radiative transfer — radio lines: galaxies

1. INTRODUCTION

OH megamasers are extremely luminous extragalactic OH maser sources that have isotropic luminosities a million or more times greater than their Galactic counterparts. OHMs are found only in the nuclear regions of luminous (LIRGs) and ultraluminous (ULIRGs) infrared galaxies, where intense star formation is occurring. These masers emit primarily in the main lines at 1667 and 1665 MHz, although weaker emission in the satellite lines at 1612 and 1720 MHz has also been detected (Baan & Haschick 1987). In addition to their immense luminosities, OHMs differ from their Galactic counterparts in their very large line widths and their 1667/1665 MHz flux ratios. Galactic OH mainline masers in star-forming regions tend to have line widths $\lesssim$1 km s^{-1} and 1667/1665 MHz flux ratios less than 1. In contrast, OHMs have overall line widths $\gtrsim$100 km s^{-1} and their 1667/1665 MHz flux ratios are always greater than 1. Although this ratio varies, the typical ratio is $\sim$5 (Lonsdale 2002). Baan (1989) found a clear separation between OH emitters and absorbers on the basis of the IR properties of the host galaxies. The OHMs have larger IR luminosity ($\mathcal{L}_{\rm IR}$) and tend to be warmer. OHMs may occur for lower $\mathcal{L}_{\rm IR}$ as long as the dust is warm enough. The Arecibo OHM survey conducted by Darling & Giovanelli (2002) targeted LIRGs and increased the number of OHMs to $\sim$100. That survey substantiated the conclusions of Baan (1989) and showed that the fraction of OHMs in LIRGs is an increasing function of far-IR (FIR) luminosity and color, with most of the detections found in warm ULIRGs. These observations strongly suggest that the masers are pumped by the intense FIR radiation in the OH pump lines at 53 μm and 35 μm. Support for FIR pumping is provided by observations using the *Infrared Space Observatory* (*ISO*). Skinner et al. (1997) observed the 35 μm pumping transition in Arp 220 and concluded that absorption in this line alone could power its maser emission. Significantly, OH and water megamasers have not been observed in the same galaxy (Lo 2005) even though both are often found in the same Galactic star-forming regions.

The standard OHM model was introduced by Baan (1985), who proposed that the maser emission is produced by low-gain, unsaturated amplification of background radio continuum. This proposal was confirmed by the comprehensive study of OHMs performed by Henkel & Wilson (1990). They found good agreement with observations if the maser transitions have approximately equal excitation temperatures, giving a 1667/1665 MHz optical depth ratio of $\sim$1.8. However, subsequent VLBI observations revealed compact maser emission on parsec scales with amplification factors $\gtrsim$800 and very large 1667/1665 MHz line ratios (Lonsdale et al. 1998). A surprise of these observations was that line widths remained large (tens of km s^{-1}) even on the smallest observed angular scales (Lonsdale 2002). The VLBI observations led to the suggestion that there are two different modes of maser operation—low-gain, unsaturated amplification responsible for the diffuse maser emission and high-gain, saturated emission producing the compact sources. It was also suggested that the two classes may have different pumping mechanisms, with the diffuse emission pumped by IR radiation and the compact masers by a combination of collisions and radiation (Lonsdale 2002). However, an extension of the standard model is able to explain both the diffuse and compact emission from III Zw 35 by assuming a clumpy maser medium (Parra et al. 2005). Each cloud generates low-gain, unsaturated emission, and strong compact emission occurs when the line of sight intersects more than one cloud. A similar model has been used to explain the megamaser emission from IRAS 17208−0014 (Momjian et al. 2006). The clumpy maser model also explains the observation that compact masers are always found embedded in the diffuse emission and do not occur in isolation (Lonsdale 2002).

[1] Centre College, 600 West Walnut Street, Danville, KY 40422; lockett@centre.edu.
[2] Physics and Astronomy, University of Kentucky, Lexington, KY 40506-0055; moshe@pa.uky.edu.

An observational difficulty is that the nearest OHMs are located at distances of $\sim$100 Mpc and thus cannot be probed nearly as accurately as Galactic masers. The study of OHMs thus relies heavily on analyzing their global properties. It is important to first explain the global properties of OHMs and then construct more comprehensive models for those sources that have been observed in more detail using VLBI techniques. Previous OHM models (Henkel & Wilson 1990; Randell et al. 1995) were performed before the discovery of the compact maser sources. Although the clumpy maser model seems to provide a phenomenological explanation to the compact and diffuse maser emissions, it is not yet backed by pumping calculations. The time is right to develop a pumping model that can explain both the compact and diffuse emission using physical conditions that are consistent with those expected in the maser regions. This is the aim of the present paper. In § 2 we summarize what is known concerning the physical conditions existing in the maser region. In § 3 we explain our model and present the results of our calculations. Section 4 contains a summary and discussion.

2. PHYSICAL CONDITIONS IN THE MASER REGION

Calculating maser intensities requires knowledge of the physical conditions existing in the maser region. The important parameters are the FIR radiation intensity, OH column density, gas density and temperature, and line width. The physical conditions in the nuclear regions of OHMs are significantly different from those found in normal galaxies due to the extreme amount of massive star formation. Although hidden from view at visible wavelengths, Lonsdale et al. (2006) have observed numerous radio point sources in the nuclear region of Arp 220 and conclude that they are radio supernovae. They deduce a supernova rate of $\sim$4 per year, yielding a per-volume rate that is orders of magnitude larger than Galactic. These radio sources have recently been observed at other radio wavelengths, and the SN nature of the sources has been strengthened (Parra et al. 2007). That study also found that an unusually large fraction of these supernovae are highly luminous, suggesting that stellar formation and evolution may be much different in these regions compared to normal galaxies. The large amount of massive star formation results in the intense FIR radiation and turbulence present in the region of maser production.

2.1. *FIR Radiation Intensity*

The intense FIR radiation field present in the nuclei of LIRGs and ULIRGs is the dominant pump for the OHMs. Estimates of the effective dust temperature and opacity have been calculated in numerous studies. The *IRAS*-derived color temperatures of 74 OHMs range from 40 to 90 K with a median of 60 K (Klöckner 2002). Yun & Carilli (2002) find best-fit dust temperatures in the range 59–72 K for the OHMs Arp 220, Mrk 273, and Mrk 231. These are global estimates and may be influenced by cooler dust lying outside the maser region. Soifer et al. (1999) performed high spatial resolution observations of the nuclear region of Arp 220 from 3 to 25 μm and conclude that the region is complicated with a range of source temperatures and sizes. They find that emission at wavelengths longer than 20 μm corresponds to a dust temperature of $\sim$85 K. This result is consistent with a detailed theoretical analysis of radiation pressure–supported starbursts, which finds the effective dust temperature to be $\sim$90 K for the optically thick starburst disks of ULIRGs (Thompson et al. 2005). A possible upper limit to the dust temperature of $\sim$100 K may be provided by the lack of observation of the 6.7 GHz methanol maser emission in OHMs (Darling et al. 2003). This methanol transition is often found to be a strong maser in association with OH masers in Galactic star-forming regions. Modeling of the 6.7 GHz maser finds that it is radiatively pumped and requires dust temperatures $\gtrsim$100 K (Cragg et al. 2005).

The dust opacity in OHMs is not constrained as tightly by observations, and the estimated opacity depends on the wavelengths being examined. Lisenfeld et al. (2000) discuss a number of arguments that suggest visual opacities of order 1000. However, other studies estimate much smaller visual opacities in the range 20–200 (Soifer et al. 1999; Hinz & Rieke 2006). It should be noted that the values of dust temperature and opacity that best fit the observed spectral energy distributions are not independent and there is considerable degeneracy between the two parameters (Blain et al. 2003).

2.2. *Gas Temperature and Molecular Density*

Gas temperature and density are needed to calculate collision rates. Although OHM pumping is dominated by radiation, collisions need to be included in the calculation of the OH level populations. It has also been suggested that the compact masers may be pumped by a combination of collisions and radiation (Lonsdale 2002). The temperature and density can be estimated using high-density tracer molecules such as HCN, CS, and HCO^+. Cernicharo et al. (2006) observed transitions in HCN and HNC in Arp 220, and their analysis predicts densities in the range 10^5–10^6 cm^{-3} and gas temperature $\sim$40 K. Greve et al. (2006) observed Arp 220 using numerous molecular lines including those of HCN, CS, and HCO^+. They deduce densities in the range 10^4–10^6 cm^{-3} and gas temperatures ranging from 50 K to 70 K. Further constraints on these parameters are provided by the lack of detection of the 22 GHz water maser combined with the detection of the 183 GHz water maser in Arp 220 (Cernicharo et al. 2006). The 22 GHz maser is collisionally pumped and requires relatively high densities and temperatures for its production. The 183 GHz maser is produced at much lower densities and temperature. Cernicharo et al. (2006) perform calculations that show that strong 183 GHz emission without 22 GHz emission requires densities $\lesssim 10^6$ cm^{-3} and gas temperatures $\lesssim$100 K.

2.3. *Line Width*

Line width usually affects the level populations only as part of the combination $n_{\rm OH}R/\Delta V$, the column density per velocity interval; neither $n_{\rm OH}$, R, nor ΔV enters separately. However, overlap between FIR rotational lines of OH introduces the line width as an independent parameter with additional, separate effects on the level populations. Line overlap affects photon trapping since a photon emitted in one transition may be absorbed in a different one. In addition, line overlap can significantly affect the absorption of the pumping radiation in the overlapping transitions. The lowest 24 hyperfine levels of OH are shown in Figure 1. The level structure is more complicated than is found for the typical diatomic molecule. There are two rotational ladders, and each rotational level is split into four sublevels due to the effects of Λ doubling and hyperfine splitting. The hyperfine separations differ in the two halves of the Λ-doublets leading to line separations as small as 0.1 km s^{-1} between FIR rotational lines. Figure 1 shows that the asymmetry is especially large for the transitions involving the $^2\Pi_{1/2}$ ladder.

An important feature of OHMs is their very large line width. Single-dish observations of OHMs reveal line widths of hundreds of km s^{-1}. Much of this line width is due to large-scale motions of individual maser clouds. However, VLBI imaging

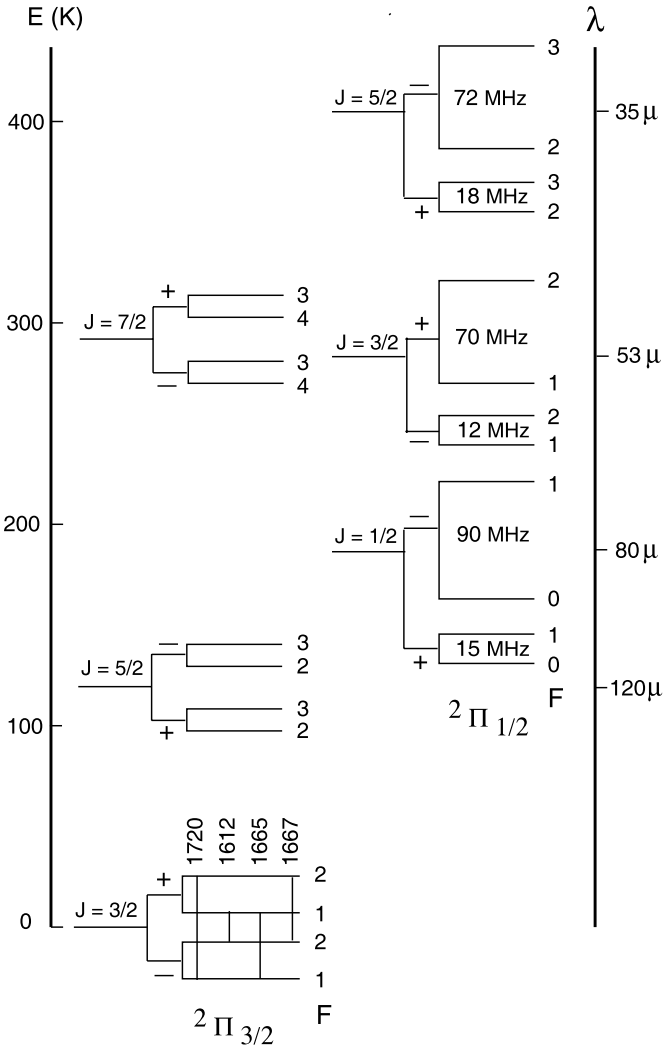

FIG. 1.—The 24 hyperfine levels of OH used in our calculations. Λ-doublet and hyperfine splitting are not to scale. Note the very uneven spacings in the Λ-doublets of the $^2\Pi_{1/2}$ ladder, which cause extremely asymmetric line overlap between the FIR lines involving these states.

finds that line widths are still tens of km s^{-1} even for parsec-size regions (Lonsdale 2002). These observations indicate the presence of a large amount of supersonic turbulence and are in agreement with the theoretical predictions of Thompson et al. (2005), who estimate turbulent line widths of $\sim$50 km s^{-1}. Downes & Solomon (1998) performed a detailed analysis of the central region of ULIRGs using CO interferometry and found that the contribution of local turbulence to the overall line width is $\gtrsim$30 km s^{-1}. Detailed modeling of the megamasers in III Zw 35 by Parra et al. (2005) found best agreement with observations using a cloud internal velocity dispersion of 20 km s^{-1}. These large line widths lead to a significant amount of overlap in the OH FIR transitions.

3. MODELING AND RESULTS

Although all four ground-state transitions have been observed as masers in OHMs, the satellite lines at 1612 MHz and 1720 MHz are much weaker than the main lines at 1667 MHz and 1665 MHz. Satellite line maser pumping follows naturally from the OH level structure, but main-line pumping requires an asymmetry in the excitation of the two halves of the Λ-doublets (Elitzur 1992). Possible asymmetric pumps include radiative pumping by warm dust or overlap between the OH FIR rotational lines. In the Appendix we discuss FIR pumping in detail and show that line overlap completely dominates all other suggested FIR pumping mechanisms of main-line masers.

We solve for the populations of the 24 levels shown in Figure 1. These include all the levels with direct radiative connection to the ground state, where the masers are produced. We have checked that increasing the number of levels makes no difference on the outcome. The statistical equilibrium equations are set in the escape probability approach using the Capriotti (1965) escape probability. This is equivalent to a slab approximated with a constant source function and should provide reasonable estimates of the overall emission from the region. Further discussion of this technique and comparison with exact radiative transfer solutions can be found in Elitzur & Asensio Ramos (2006). As noted in § 2.3, the OH energy level structure necessitates inclusion of the effects of line overlap. We use the method of Lockett & Elitzur (1989) to treat the local overlap of the FIR rotational lines. This procedure is based on the slab escape probability method and accounts for overlap effects by numerically integrating the amount of absorption in the overlapping lines assuming Gaussian line profiles. This method is similar to that of Guilloteau et al. (1981) except they assume a spherical geometry as opposed to a slab.

We envision the maser source embedded in a dusty environment that provides the pumping IR radiation. Assuming the dust temperature T_d to be approximately uniform across the maser cloud, the local radiation field can be described with

$$I_\nu = B_\nu(T_d)(1 - e^{-\tau_\nu}). \quad (1)$$

Here $B_\nu(T_d)$ is the Planck function and τ_ν is the frequency-dependent dust opacity across the region where its temperature can be described by the single value T_d. Note that τ_ν is the dust optical depth over the entire dusty region and can be larger than its value across the maser cloud. The spectral shape of τ_ν is found using the cross sections of Draine & Lee (1984).

Although radiation is the dominant pumping mechanism, collisions need to be included in the calculations, and we utilize the most recent collision rates from Offer et al. (1994). These rates are considerably different for collisions with ortho and para H_2, and the pumping could depend sensitively on the ortho-para ratio (Lockett et al. 1999). This ratio is uncertain in molecular clouds. H_2 is believed to form with the ortho-para ratio $\sim$3, and the ratio approaches thermal equilibrium at a rate depending on the chemical history of the cloud (Flower 1990). We performed calculations ranging from pure ortho to pure para and the results did not vary significantly. Our nominal choice for the ortho-para ratio is 1, which is the equilibrium value for $T \sim 77$ K.

We explored a wide range of the physical parameters and found a large volume of phase space where the main lines are inverted. Table 1 lists the values of the parameters we consider "standard." We now present our results, varying the model parameters one at a time from these nominal values.

3.1. *Effects of Dust Temperature and Opacity*

Figure 2 plots the contours of 1667 MHz negative optical depth versus dust temperature and opacity. A minimum dust temperature of about 45 K is needed for maser production, and maximum maser inversion occurs for dust temperatures between 80 and 140 K for the expected range of dust opacity. When the dust opacity becomes very large, the dust radiation approaches that of a blackbody and the maser begins to thermalize. Beyond a visual opacity of about 300 there is little dependence of maser strength on dust temperature. There is also a minimum FIR pumping flux needed for maser production,

TABLE 1
"STANDARD" MODEL PARAMETERS

Parameter	Value
Dust temperature, T_d	60 K
Dust optical depth at visual	100
Line width (FWHM), ΔV	20 km s^{-1}
OH column density, $n_{OH}R$	6×10^{16} cm^{-2}
Gas temperature	50 K
Gas density	10^4 cm^{-3}

NOTES.—The parameters were chosen to be representative of individual clouds in the clumpy OHM model of Parra et al. (2005). Figures show the effects of varying individual parameters from these nominal values, as indicated in the corresponding legends.

which is a function of dust temperature. The pumping flux in equation (1) is determined by the product of two factors: the Planck function, which depends on dust temperature, and the self-absorption factor, which depends on the dust opacity at the pumping frequency. The FIR flux is increased by increasing either the dust temperature or opacity. Figure 3 shows the minimum 53 μm flux needed for inversion as a function of dust temperature. A larger flux is needed for a lower dust temperature, indicating that the FIR spectral shape is important for maser pumping. Thus a smaller $\mathcal{L}_{IR}$ can support inversion, as long as the temperature is warm enough. This agrees with the observations of Baan (1989) and Darling & Giovanelli (2002). Our analysis also shows that a minimum dust temperature is needed for inversion. Below 50 K, the Planck function at 53 μm decreases very rapidly as dust temperature decreases. The flux can be increased by increasing dust opacity, but it cannot exceed blackbody emission, and the needed flux cannot be produced for dust temperatures below about 45 K.

The pumping is primarily by the 53 μm lines, with the 35 μm transitions in a secondary role. Increasing the number of OH energy levels in the model calculations, main line inversion was not produced until the $^2\Pi_{1/2}(J = 3/2)$ levels, at 53 μm, were included. The 53 μm lines dominate the pumping, but the maser strength increased further when the four levels of $^2\Pi_{1/2}(J = 5/2)$, at 35 μm, were added. We find the opacity of the 53 μm lines to be about 5 times those of the 35 μm lines. This agrees with the

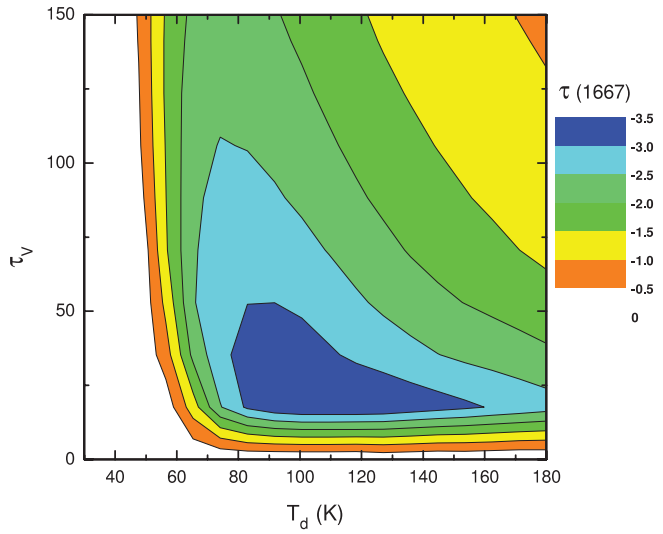

FIG. 2.—Contour plots of the inverted 1667 MHz optical depth vs. dust temperature and optical depth. All other model parameters are as listed in Table 1.

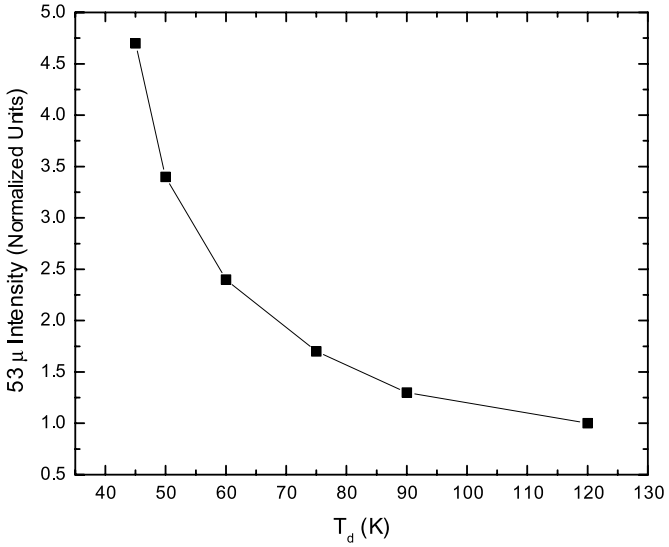

FIG. 3.—Minimal 53 μm intensity required for inversion—cooler dust requires larger minimal flux. At a given dust temperature, the plotted intensity corresponds to the minimal τ_V that produces maser inversion (see eq. [1]). Results are normalized to the minimal intensity when $T_d = 120$ K (1.08×10^{-12} ergs cm^{-2} s^{-1} Hz^{-1} sr^{-1}). Model parameters are in Table 1.

study of He & Chen (2004), who compared the line strengths in Arp 220 and found the amount of absorption in the 53 μm line to be about 6 times that of the 35 μm line. Results were hardly affected by inclusion of the $^2\Pi_{3/2}(J = 7/2)$ levels, as expected since these levels are radiatively disconnected from the ground state.

An important observed correlation is the increase of $\mathcal{L}_{OH}$ with $\mathcal{L}_{IR}$. Early OHM observations revealed an approximately quadratic relation between the two (Baan 1989), but subsequent studies using a much larger sample and taking into account Malmquist bias established the flatter dependence $L_{OH} \propto L_{IR}^{1.2}$ (Darling & Giovanelli 2002). A linear relation is expected because low-gain amplification of background radio continuum implies that $\mathcal{L}_{OH}$ is proportional to the radio luminosity, which in turn is proportional to $\mathcal{L}_{IR}$ over the relevant luminosity range (Darling & Giovanelli 2002). This linear proportionality will not be altered by the expected variations among different sources in OH covering factor of the radio continuum, which will only induce a scatter around it. Since the observed correlation is steeper than linear, Baan (1989) conjectured that maser optical depth τ_{maser} also varies linearly with the pump luminosity $\mathcal{L}_{IR}$. However, our calculations show that, depending on the different parameters, τ_{maser} in fact can either increase or decrease with the IR luminosity. Indeed, in their extensive study of OHMs, Henkel & Wilson (1990) did not find a correlation between $\mathcal{L}_{IR}$ and τ_{maser}. A possible explanation for the increase of $\mathcal{L}_{OH}$ in excess of linear proportion to $\mathcal{L}_{IR}$ may be provided by the study of HCN emission from LIRGs by Gao & Solomon (2004). They find that $\mathcal{L}_{IR} \propto \mathcal{L}_{HCN}$ and conclude that the amount of dense ($n_{H_2} \gtrsim 10^4$ cm^{-3}) molecular gas, which is traced by the HCN, is linearly proportional to $\mathcal{L}_{IR}$. It is thus reasonable to assume that, together with the increase of dense molecular gas, the number of OH maser clouds is also increasing with $\mathcal{L}_{IR}$.

Lo (2005) pointed out that, on the basis of its FIR color and $\mathcal{L}_{IR}$ the ULIRG NGC 6240 should be an OHM (see also Fig. 2 of Baan 1989). A possible reason why it is not is its low ratio of $\mathcal{L}_{IR}$ to dense molecular gas. This gas is traced by HCN and HCO^+ molecules, and Table 1 in Graciá-Carpio et al. (2006) shows that the ratios $\mathcal{L}_{IR}/\mathcal{L}_{HCN}$ and $\mathcal{L}_{IR}/\mathcal{L}_{HCO^+}$ are both less than half

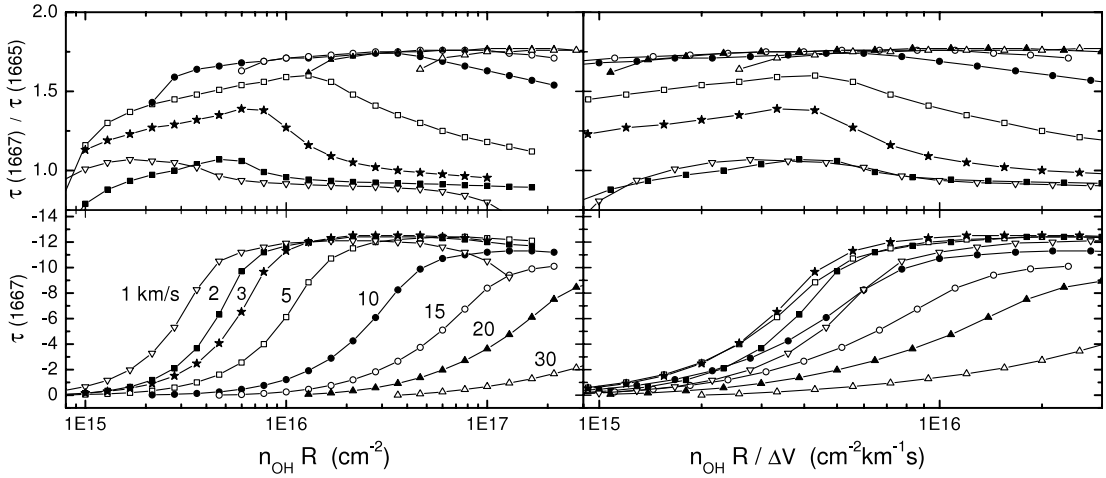

FIG. 4.— 1667 MHz optical depth and 1667/1665 MHz optical depth ratio for different line widths. Left panel is plotted vs. OH column density. Right panel is plotted vs. OH column density per velocity interval. All other model parameters are from Table 1. Note that line widths $\lesssim$2 km s^{-1} lead to 1667/1665 MHz optical depth ratios $\lesssim$1, while line widths $\gtrsim$3 km s^{-1} cause this ratio to increase dramatically, becoming $\sim$1.75 for line widths $\gtrsim$10 km s^{-1}.

in NGC 6240 than in every OHM, seven in all, included in their sample. Thus, the FIR pump rate per molecule in NGC 6240 is much lower than in the typical OHM. Therefore, a minimum ratio of pumping radiation to dense molecular gas may also be a prerequisite for producing OHMs. Darling (2007) has recently conducted a detailed study that shows a clear separation between OHMs and OH absorbers based on the amount of dense molecular gas.

3.2. *Effects of Collisions*

We found no conditions where collisions alone produce the observed maser emission. When combined with a strong FIR radiation field, collisions tend to weaken and then thermalize the masers. Increasing the collision rate by increasing either gas temperature or density tends to reduce the maser strength. An increase in the collision rate also increases the dust temperature required for inversion—increasing the density from 10^4 to 10^5 cm^{-3} raises the minimal dust temperature from about 45 K to 50 K. These results argue against collisional pumping as a source of the compact masers. Another argument against collisional pumping is the absence of the 22 GHz water maser combined with the presence of the 183 GHz water maser in Arp 220. We calculated the level populations for ortho and para water for conditions representative of the OHM region, and our results are consistent with those of Cernicharo et al. (2006). The presence of the 183 GHz maser combined with the absence of the 22 GHz maser implies densities $\lesssim 10^6$ cm^{-3} and temperature $\lesssim$100 K. These conditions are not conducive to collisional pumping of the OHM.

3.3. *Effects of Line Overlap*

We find that the effects of line overlap dominate the main-line inversion even at line widths as small as 0.5 km s^{-1}. In the Appendix we discuss FIR pumping in detail and show that line overlap completely dominates all other suggested FIR pumping mechanisms of main-line masers. Calculations that do not include overlap effects cannot produce reliable results for FIR pumping.

Figure 4 shows the effects of line overlap on the 1667 MHz maser strength and the 1667/1665 MHz optical depth ratio. Because optical depth is determined by the column density per velocity interval, $n_{\rm OH}R/\Delta V$ remains a scaling variable, as is evident from the figure's right panels; they show that the pumping results display similar behavior for the different line widths when plotted in terms of this variable. Line overlap effects add ΔV as another independent parameter of the pump scheme, with striking effects on the inversion: the model results for the ratio $R = \tau(1667)/\tau(1665)$ split into two groups, with a sharp transition between the two. Starting from $\Delta V = 2$ km s^{-1}, a decrease of 1 km s^{-1} has little effect on R while an increase of 1 km s^{-1} increases R significantly, especially at the lower end of column densities. Line widths $\gtrsim$10 km s^{-1} have $R \simeq 1.8$ independent of ΔV. All ground-state hyperfine transitions are then inverted with approximately the same excitation temperature, an equality that was also noted by Henkel & Wilson (1990). In contrast, line widths $\lesssim$2 km s^{-1} produce $R \lesssim 1$, again displaying behavior that is nearly independent of ΔV. Further discussion of this behavior is provided in the Appendix.

Our results can explain why the flux ratios observed for OHMs differ radically from those found for their Galactic counterparts. Galactic interstellar masers tend to have small line widths and the 1665 MHz line is usually the strongest, with the strength of the 1667 MHz line often comparable to that of the satellite lines (Gaume & Mutel 1987). However, there are exceptions where the 1667 MHz line or one of the satellite lines is the strongest. Our results show that this is the expected behavior for $\Delta V \lesssim 2$ km s^{-1}. In contrast, in OHMs the 1667 MHz line is always the strongest and the satellite lines are much weaker by factors $\gtrsim$10, the expected behavior when $\Delta V \gtrsim 10$ km s^{-1}. Significantly, main-line masers in OH/IR stars tend to have larger line widths than Galactic interstellar masers and their 1667/1665 MHz flux ratios tend to be larger than 1.

We find that all ground-state transitions are inverted with approximately equal excitation temperatures when $\Delta V \gtrsim 10$ km s^{-1}. This is consistent with the OHMs global fluxes determined from observations (Henkel & Wilson 1990). The optical depth of the 1667 MHz line is then $\sim$1.8 times that of the 1665 MHz line and $\sim$9 times that of the satellite lines, and the fluxes for the OH maser amplified background continuum become functions of optical depth alone. Figure 5 displays the amplified 1665, 1667, and 1720 MHz line fluxes. Because of its stronger amplification, at a given instrumental sensitivity the 1667 line will be detected over the largest portion of a source. The 1667/1665 MHz and 1667/1720 MHz flux ratios increase as the 1667 MHz maser gets stronger. Small optical depths give a 1667/1665 MHz flux ratio of $\sim$2, and the typically observed ratio of 5 implies that the magnitude of $\tau(1667)$ is $\sim$3.5. Because the 1720 MHz is so weak

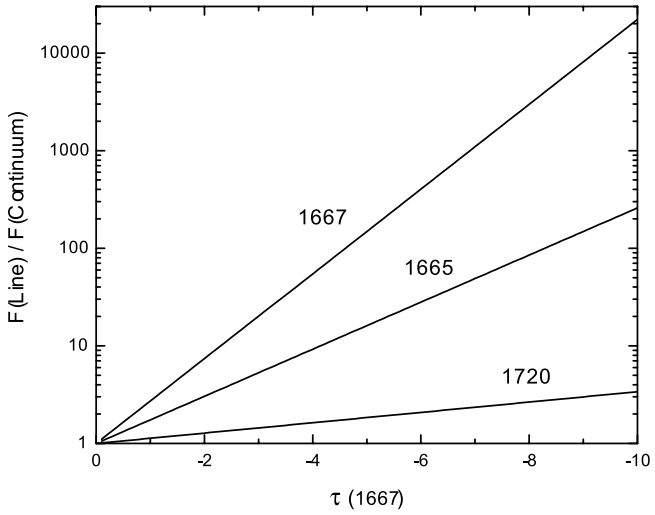

FIG. 5.— Variation of flux with 1667 MHz optical depth for the three indicated masers when all ground-state transitions have the same excitation temperature (the situation when $\Delta v \gtrsim 10$ km s^{-1}; see § 3.3). The 1667/1665 and 1667/1720 flux ratios increase as the 1667 MHz maser gets stronger. The typically observed 1667/1665 MHz flux ratio of 5 implies $\tau(1667) \approx -3.5$, and the 1720 MHz line will always be weak compared to the 1667 MHz line.

compared to the 1667 MHz line, its detection is limited. Figure 6 plots the track of 1667/1720 MHz flux ratio versus the 1667/1665 MHz flux ratio as $\tau(1667)$ is varied. Also shown are the data for four relatively nearby OHMs, taken from Baan et al. (1989, 1992) and Martin et al. (1989). The agreement is surprisingly good considering the large uncertainties in the data.

3.4. *Clumpy OHM*

The global properties of OHMs are consistent with the standard model of low-gain amplification of background radiation with the maser transitions having approximately equal excitation temperatures. Compact, bright maser emission is explained by the clumpy nature of the amplifying medium. Each maser cloud produces low-gain, unsaturated emission. Compact emission would be observed when the line of sight intersects a number of maser clouds. This model has been used to give very good agreement with the maser emission from III Zw 35. Pihlström et al. (2001) observed III Zw 35 using intermediate and high resolution and detected both diffuse and compact emission. They proposed a model based on a clumpy maser medium located in a rotating ring. This model was extensively improved by Parra et al. (2005), who used Monte Carlo simulations to account for the overlap of individual maser clouds. The clumpy maser model gives results that are in excellent agreement with the observed spectra and with interferometric observations on all angular scales. The compact maser emission arises at the tangents to the ring where cloud overlap is greatest in both position and velocity. The model of III Zw 35 finds best agreement with observations using maser clouds having a size $\lesssim 0.7$ pc, magnitude of $\tau(1667) \sim 1.5$, and velocity dispersion of ~ 20 km s^{-1}. A similar, but less detailed, model has since been developed to explain the compact and diffuse emission from IRAS 17208−0014 (Momjian et al. 2006).

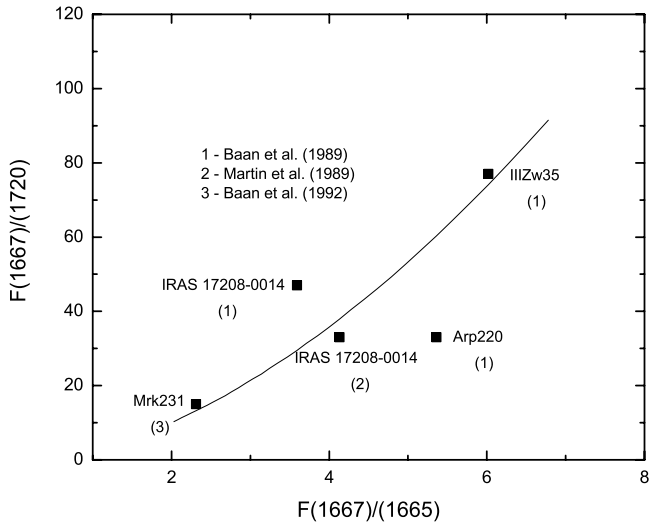

FIG. 6.— "Color-color" diagram for OH maser lines. Filled squares show data points for four OHMs. The solid line is the track of flux ratios of the amplified background continuum when all lines have the same excitation temperature. The 1667 MHz optical depth varies along the track from −0.5 at the lower left to −4 at the upper right.

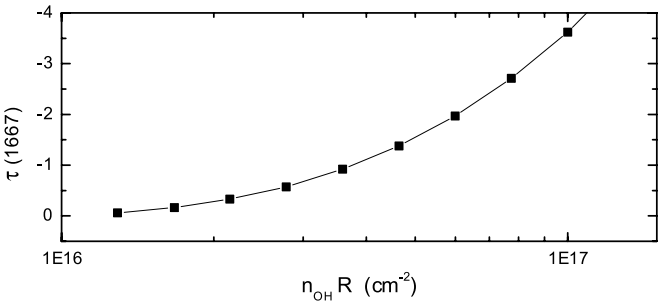

FIG. 7.— 1667 MHz maser optical depth for an OHM cloud using the model parameters from Table 1. This is a zoom in on the relevant portion of figure 4. The optical depth of −1.5 for OH column density of $\sim 5 \times 10^{16}$ cm^{-2} is in good agreement with the requirements of the clumpy model of OHM emission in III Zw 35 (see § 3.4).

Our "standard" parameters in Table 1 were selected to match the III Zw 35 model results of Parra et al. (2005). Figure 7 is an expanded view of the relevant portion in Figure 4 and shows that the magnitude of $\tau(1667)$ is about 1.5 at an OH column density of $\sim 5 \times 10^{16}$ cm^{-2}. With the model density of 10^4 cm^{-3}, this implies an OH abundance of $\sim 2 \times 10^{-6}$ for the cloud size of 0.7 pc. Calculated OH column densities are typically in the range 10^{15}–10^{16} cm^{-2} for both PDRs (Hartquist & Sternberg 1991) and C-shocks (Wardle 1999). Larger OH column densities may be obtained through other mechanisms such as the photodissociation of water produced from the evaporation from grain mantles (Hartquist et al. 1995). However, even that mechanism has an upper limit of $\sim 10^{17}$ cm^{-2}. Figure 4 shows that very large 1667 MHz optical depths can be produced, but only if ΔV is $\lesssim 20$ km s^{-1} or the OH column exceeds $\sim 10^{17}$ cm^{-2}. Neither condition is likely to be met in OHMs. Maser amplification by single clouds is weak because line widths are large ($\gtrsim 20$ km s^{-1}) and OH columns are limited to $\lesssim 10^{17}$ cm^{-2}.

The clumpy maser model can also be used to explain the lack of compact maser emission from Mrk 231. This is the only OHM examined with VLBI not to exhibit compact emission (Lonsdale et al. 2003). Furthermore, the 1667/1665 MHz flux ratio has been found to be ~ 2 on angular scales ranging over 3 orders of magnitude (Richards et al. 2005; Klöckner et al. 2003). These observations are consistent with the main lines having similar excitation temperatures while undergoing low-gain amplification. Speculative explanations for the lack of compact emission have been proposed (Lonsdale et al. 2003), but a simpler explanation is based on the geometry of a rotating

clumpy maser disk. Richards et al. (2005) and Klöckner et al. (2003) each propose that the masers are produced in a rotating disk that is more inclined to the line of sight than is found for OHMs such as III Zw 35. The length along the line of sight through the disk is thus smaller than if the disk were observed edge on, resulting in little cloud overlap and no compact emission. Richards et al. (2005) estimate maser cloud sizes $\sim$1 pc with the magnitude of $\tau(1667)$ about 1. These estimates are comparable to the values suggested by Parra et al. (2005) in their detailed analysis of III Zw 35.

4. SUMMARY AND DISCUSSION

OHMs are characterized by their extreme luminosity, 1667/1665 MHz flux ratio greater than 1, and large line widths. Our detailed pumping analysis of OHMs shows that the above properties are a natural outcome of an intense FIR pump combined with line overlap effects due to large turbulent line widths. The 53 μm lines provide the primary pump, and a minimum dust temperature of $\sim$45 K is needed for main-line maser production. In agreement with the observations of Baan (1989) and Darling & Giovanelli (2002) we find that a smaller $\mathcal{L}_{\rm IR}$ can support inversion, as long as the temperature is warm enough. We find no conditions where collisions can produce the observed maser emission, and when combined with a strong FIR radiation field, collisions tend to weaken and then thermalize the masers. These results are consistent with the detection of the 183 GHz water maser combined with the lack of detection of the 22 GHz water maser in Arp 220 (Cernicharo et al. 2006). The 22 GHz maser is collisionally pumped and requires relatively high densities and temperatures for its production, while the 183 GHz maser is produced at much lower densities and temperature. The large OHM line widths produce significant overlap among the the 53 μm pump lines resulting in nearly equal negative excitation temperatures for all ground-state transitions, in agreement with observations (Fig. 6; see also Henkel & Wilson 1990). The 1667/1665 MHz flux ratios are thus greater than 1 and only weak satellite line emission is produced. Our pumping results are in agreement with those required by clumpy maser models that explain both the diffuse and compact maser emission from OHMs such as III Zw 35. Finally, the small observed ratios of $\mathcal{L}_{\rm IR}/\mathcal{L}_{\rm HCN}$ and $\mathcal{L}_{\rm IR}/\mathcal{L}_{\rm HCO^+}$ relative to those found in OHMs is a possible reason for the lack of OH megamaser emission in the ULIRG NGC 6240. A minimum ratio of pumping radiation to dense molecular gas may be a prerequisite for becoming a OHM.

Excited state transitions at 5 cm and 6 cm have also been observed in OHMs. However, these lines have been detected only in absorption. Henkel et al. (1987) observed absorption in the three 6 cm $^2\Pi_{1/2}(J = 1/2)$ transitions in five OHMs, and absorption has been detected also in one 5 cm $^2\Pi_{3/2}(J = 5/2)$ transition in Arp 220 (Henkel et al. 1986). These observations are surprising since masing in the 5 cm and 6 cm lines has often been observed in conjunction with Galactic ground-state OH maser sources (Cesaroni & Walmsley 1991). Our pumping models of ground-state maser emission in OHMs usually predict absorption in the 5 cm lines. However, the 6 cm lines are weakly inverted with opacities a hundred times smaller than the 1667 MHz line. Our calculations find that absorption in the 6 cm lines requires smaller dust temperatures than exist in the maser regions. We expect the absorption to occur outside the maser regions where the dust temperature is lower. Understanding the absorption at 5 cm and 6 cm is an important problem that we plan to treat in a future paper.

4.1. *OH Main-Line Maser Pump*

Our results suggest that *all* OH main-line masers could be pumped by the same mechanism: far-IR radiation. The major differences between Galactic star-forming regions on one hand and evolved stars and OHMs on the other can be attributed to differences in line overlap effects. As shown in § 3.3, line width is the most important factor in determining the 1667/1665 MHz flux ratio and thus is the dominant factor causing the extreme differences between the flux ratios of the two classes. In Galactic star-forming regions the observed line widths are $\lesssim$1 km s^{-1} and the 1665 MHz maser is usually strongest, with the 1667 MHz line often comparable in strength to the satellite lines. In OHMs the line widths are large ($\gtrsim$10 km s^{-1}) and the 1667 MHz line is always stronger than the 1665 MHz line, with the satellite lines much weaker. Our results show that such large line widths produce approximately equal negative excitation temperatures for the four ground-state transitions, resulting in the 1667 MHz line being stronger than the 1665 MHz line and much weaker satellite lines. Smaller line widths tend to produce a stronger inversion in the 1665 MHz line. In evolved stars, the main-line maser velocities are larger than those found in Galactic star-forming regions, and they also tend to have 1667/1665 MHz flux ratios $\gtrsim$1. Thus, the line width could be the main reason why OH main-line masers display differences in spite of sharing a common pump mechanism.

Partial support by NSF grant AST-0507421 (M. E.) is gratefully acknowledged.

APPENDIX

MAIN-LINE PUMPING BY FIR RADIATION

Pumping of the ground-state main-line masers at 1667 and 1665 MHz requires asymmetry in the excitation of the two halves of the Λ-doublets. The main ingredients of the pump analysis are as follows:

1. Most molecules are in the ground state, from which they are excited into higher levels and cascade back to the ground.
2. Downward transitions are due to radiative decays. For each level on the $^2\Pi_{1/2}$ ladder, the strongest decay is always down the ladder. Thus the cascade proceeds primarily along the $^2\Pi_{1/2}$ ladder, until the final decay $^2\Pi_{1/2}(J = 1/2) \rightarrow ^2\Pi_{3/2}(J = 3/2)$. Pumps that rely on cross-ladder transitions are thus inherently weak.
3. Line overlap modifies the fundamental radiative transition rates, making the FIR pump cycle more conducive to asymmetries.

The last point is especially important. In the absence of overlap, the escape probability approximation for the radiative rate is $A\beta$, where A and β are, respectively, the transition A-coefficient and the escape probability. For optically thick transitions, $A\beta \simeq A/\tau$, and the radiative decay rates then become independent of line strength. The distinctions between different transitions disappear in this case, making it difficult to maintain any asymmetry required for inversion. This is no longer true in the presence of line overlap. The transition rate now depends on the strengths of all overlapping lines in a complex way that involves also the degree of overlap. The

distinctions between different transitions are maintained over a much larger range of column densities, creating the possibility for a stronger maser effect.

FIR main-line pumping is dominated by line overlap effects, primarily in the 53 μm pump. On the $^2\Pi_{3/2}$ ladder, the hyperfine splits are roughly equal in the two halves of the Λ-doublet. But on the $^2\Pi_{1/2}$ ladder, the hyperfine split of the upper half of each Λ-doublet is larger than in the lower half by factors of 4–6 (see Fig. 1). These uneven splits create an asymmetry in the overlap of the pump lines connecting the ground state to the rotational states of the $^2\Pi_{1/2}$ ladder. In contrast, there is essentially no overlap asymmetry in the image transitions for the 120 μm pump lines connecting the ground state to the the first excited state in the $^2\Pi_{3/2}$ ladder. The 53 μm pump lines have special properties because they populate the $^2\Pi_{1/2}(J = 3/2)$ state, whose quantum numbers directly mirror the ground state. This places it in a special position during both the excitation and cascade phases. First, the 53 μm pump cycle is the only one in which each upper level connects to the two ground-state levels in the appropriate Λ-doublet; in all other cases, one of the excited rotational levels has only one transition to the ground because of the dipole selection rules. This doubles the number of potential overlaps compared to the other cycles, creating more asymmetry during the excitation phase of the pump cycle. Second, barring cross-ladder transitions, this is the only pump cycle that shuffles the molecules between the two halves of the ground-state Λ-doublet. In contrast, both the 80 μm and the 35 μm pump cycles return the molecules into the very same Λ-doublet from which they started.

The large efficiency of the 53 μm pump is produced by asymmetric overlap effects on both the absorption rates out of the ground-state levels and the returning decays. The inverting effects of line overlap on the absorption rates were first noted by Burdyuzha & Varshalovich (1973) and applied to OHMs by Burdyuzha & Vikulov (1990). They found that the smaller amount of overlap between the 53 μm pump lines out of the lower Λ-doublet of the ground state reduces the shielding from the pumping dust radiation and thus increases the pumping out of the lower Λ-doublet relative to that from the upper. Burdyuzha & Vikulov (1990) used a fixed Doppler width of 0.7 km s^{-1} and found the 1667/1665 MHz flux ratio to be $\sim$1, in agreement with our results.

The asymmetries of the radiative excitations disappear when $\Delta V \gtrsim 10$ km s^{-1} because there is then complete overlap of the 53 μm lines. However, the inversion is sustained at larger line widths due to overlap effects in the cascade back to the ground. Overlaps among the $^2\Pi_{1/2}(J = 3/2) \rightarrow {}^2\Pi_{1/2}(J = 1/2)$ cascades are particularly important since they are the primary decay routes out of the upper rotational state of the 53 μm pump. In addition, the overlap asymmetry between the two halves of these Λ-doublets is extreme. The separations between the transitions connecting the lower doublets range from 0.5 to 2.5 km s^{-1}, while the corresponding transitions between the upper doublets have separations ranging from 3.3 to 15 km s^{-1}, a factor of 6 larger. The line overlap asymmetry in these transitions remains important for very large line widths. The overlap of these lines significantly enhances the 53 μm pump efficiency and is necessary to invert the ground-state Λ-doublets for line widths $\gtrsim$10 km s^{-1}.

When the line widths exceed $\sim$40 km s^{-1} the asymmetries in the cascade transitions disappear, too, and the ground-state lines thermalize. It may be noted that the calculations of Burdyuzha & Vikulov (1990) did not produce inversions at $\Delta V \gtrsim 5$ km s^{-1} because they neglected overlap effects in the decays. In contrast, we include all possible overlaps, which essentially involve *every* FIR transition when $\Delta V \gtrsim 10$ km s^{-1}.

REFERENCES

Baan, W. A. 1985, Nature, 315, 26
———. 1989, ApJ, 338, 804
Baan, W. A., & Haschick, A. D. 1987, ApJ, 318, 139
Baan, W. A., Haschick, A. D., & Henkel, C. 1989, ApJ, 346, 680
———. 1992, AJ, 103, 728
Blain, A. W., Barnard, V. E., & Chapman, S. C. 2003, MNRAS, 338, 733
Burdyuzha, V. V., & Varshalovich, D. A. 1973, Soviet Astron., 17, 308
Burdyuzha, V. V., & Vikulov, K. A. 1990, MNRAS, 244, 86
Capriotti, E. R. 1965, ApJ, 142, 1101
Cernicharo, J., Pardo, J. R., & Weiss, A. 2006, ApJ, 646, L49
Cesaroni, R., & Walmsley, C. M. 1991, A&A, 241, 537
Cragg, D. M., Sobolev, A. M., & Godfrey, P. D. 2005, MNRAS, 360, 533
Darling, J. 2007, ApJ, 669, L9
Darling, J., & Giovanelli, R. 2002, AJ, 124, 100
Darling, J., Goldsmith, P., Li, D., & Giovanelli, R. 2003, AJ, 125, 1177
Downes, D., & Solomon, P. M. 1998, ApJ, 507, 615
Draine, B. T., & Lee, H. M. 1984, ApJ, 285, 89
Elitzur, M. 1992, Astronomical Masers (Dordrecht: Kluwer)
Elitzur, M., & Asensio Ramos, A. 2006, MNRAS, 365, 779
Flower, D. 1990, Molecular Collisions in the Interstellar Medium (Cambridge: Cambridge Univ. Press)
Gao, Y., & Solomon, P. M. 2004, ApJ, 606, 271
Gaume, R. A., & Mutel, R. L. 1987, ApJS, 65, 193
Graciá-Carpio, J., García-Burillo, S., Planesas, P., & Colina, L. 2006, ApJ, 640, L135
Greve, T. R., Papadopoulos, P. P., Gao, Y., & Radford, S. J. E. 2006, preprint (astro-ph/0610378)
Guilloteau, S., Lucas, R., & Omont, A. 1981, A&A, 97, 347
Hartquist, T. W., Menten, K. M., Lepp, S., & Dalgarno, A. 1995, MNRAS, 272, 184
Hartquist, T. W., & Sternberg, A. 1991, MNRAS, 248, 48
He, J. H., & Chen, P. S. 2004, NewA, 9, 545
Henkel, C., Guesten, R., & Baan, W. A. 1987, A&A, 185, 14
Henkel, C., Guesten, R., & Batrla, W. 1986, A&A, 168, L13
Henkel, C., & Wilson, T. L. 1990, A&A, 229, 431
Hinz, J. L., & Rieke, G. H. 2006, ApJ, 646, 872
Klöckner, H.-R. 2002, Ph.D. thesis, Rijksuniversiteit, Groningen
Klöckner, H.-R., Baan, W. A., & Garrett, M. A. 2003, Nature, 421, 821
Lisenfeld, U., Isaak, K. G., & Hills, R. 2000, MNRAS, 312, 433
Lo, K. Y. 2005, ARA&A, 43, 625
Lockett, P., & Elitzur, M. 1989, ApJ, 344, 525
Lockett, P., Gauthier, E., & Elitzur, M. 1999, ApJ, 511, 235
Lonsdale, C. J. 2002, in IAU Symp. 206, Cosmic Masers: From Proto-Stars to Black Holes, ed. V. Migenes & M. J. Reid (San Francisco: ASP), 413
Lonsdale, C. J., Diamond, P. J., Thrall, H., Smith, H. E., & Lonsdale, C. J. 2006, ApJ, 647, 185
Lonsdale, C. J., Lonsdale, C. J., Diamond, P. J., & Smith, H. E. 1998, ApJ, 493, L13
Lonsdale, C. J., Lonsdale, C. J., Smith, H. E., & Diamond, P. J. 2003, ApJ, 592, 804
Martin, J. M., Le Squeren, A. M., Bottinelli, L., Gouguenheim, L., & Dennefeld, M. 1989, A&A, 208, 39
Momjian, E., Romney, J. D., Carilli, C. L., & Troland, T. H. 2006, ApJ, 653, 1172
Offer, A. R., van Hemert, M. C., & van Dishoeck, E. F. 1994, J. Chem. Phys., 100, 362
Parra, R., Conway, J. E., Diamond, P. J., Thrall, H., Lonsdale, C. J., Lonsdale, C. J., & Smith, H. E. 2007, ApJ, 659, 314
Parra, R., Conway, J. E., Elitzur, M., & Pihlström, Y. M. 2005, A&A, 443, 383
Pihlström, Y. M., Conway, J. E., Booth, R. S., Diamond, P. J., & Polatidis, A. G. 2001, A&A, 377, 413
Randell, J., Field, D., Jones, K. N., Yates, J. A., & Gray, M. D. 1995, A&A, 300, 659
Richards, A. M. S., Knapen, J. H., Yates, J. A., Cohen, R. J., Collett, J. L., Wright, M. M., Gray, M. D., & Field, D. 2005, MNRAS, 364, 353
Skinner, C. J., Smith, H. A., Sturm, E., Barlow, M. J., Cohen, R. J., & Stacey, G. J. 1997, Nature, 386, 472
Soifer, B. T., Neugebauer, G., Matthews, K., Becklin, E. E., Ressler, M., Werner, M. W., Weinberger, A. J., & Egami, E. 1999, ApJ, 513, 207
Thompson, T. A., Quataert, E., & Murray, N. 2005, ApJ, 630, 167
Wardle, M. 1999, ApJ, 525, L101
Yun, M. S., & Carilli, C. L. 2002, ApJ, 568, 88